

# Geophysical Research Letters

## RESEARCH LETTER

10.1029/2020GL087682

### Key Points:

- The Goddard Earth Observing System global circulation model is evaluated across a wide spectrum of horizontal resolution
- Across scales, the convective precipitation smoothly transitions from mostly produced by subgrid- to grid-scale model formulations
- Contrary to current views, poorer results occur when scale-aware deep convection parameterization is avoided at grid spacings of a few kilometers

### Supporting Information:

- Supporting Information S1
- Figure S1
- Figure S2
- Figure S3
- Figure S4
- Figure S5

### Correspondence to:

S. R. Freitas,  
saulo.r.freitas@nasa.gov

### Citation:

Freitas, S. R., Putman, W. M., Arnold, N. P., Adams, D. K., & Grell, G. A. (2020). Cascading toward a kilometer-scale GCM: Impacts of a scale-aware convection parameterization in the Goddard Earth Observing System GCM. *Geophysical Research Letters*, 47, e2020GL087682. <https://doi.org/10.1029/2020GL087682>

Received 5 MAY 2020

Accepted 14 AUG 2020

Accepted article online 21 AUG 2020

## Cascading Toward a Kilometer-Scale GCM: Impacts of a Scale-Aware Convection Parameterization in the Goddard Earth Observing System GCM

**Saulo R. Freitas<sup>1,2</sup> , William M. Putman<sup>2</sup>, Nathan P. Arnold<sup>2</sup> , David K. Adams<sup>3</sup> , and Georg A. Grell<sup>4</sup>**

<sup>1</sup>Goddard Earth Sciences Technology and Research, Universities Space Research Association, Columbia, MD, USA,

<sup>2</sup>Global Modeling and Assimilation Office, NASA Goddard Space Flight Center, Greenbelt, MD, USA, <sup>3</sup>Centro de Ciencias de la Atmósfera, UNAM, Mexico City, Mexico, <sup>4</sup>Earth System Research Laboratory, National Oceanic and Atmospheric Administration, Boulder, CO, USA

**Abstract** The National Aeronautics and Space Administration (NASA) Goddard Earth Observing System global circulation model (GCM) is evaluated through a cascade of simulations with increasing horizontal resolution. This model employs a nonhydrostatic dynamical core and includes a scale-aware, deep convection parameterization (DPCP). The 40-day simulations at six resolutions (100 km to 3 km) with unvarying model formulation were produced. At the highest resolution, extreme experiments were carried out: one with no DPCP and one with its scale awareness eliminated. Simulated precipitation, radiative balance, and atmospheric thermodynamic and dynamical variables are well reproduced with respect to both observational and reanalysis data. As model resolution increases, the convective precipitation smoothly transitions from being mostly produced by the convection parameterization to the cloud microphysics parameterization. However, contrary to current thought, these extreme cases argue for maintaining, to some extent, the scale-aware DPCP even at 3-km scale, as the run relying solely on explicit grid-scale production of rainfall performs more poorly at this resolution.

**Plain Language Summary** Global circulation models (GCMs) are the means we have to predict the weather and assess the future climate on daily, seasonal, and even century-long timescales. GCMs are computational tools that employ approximate forms of the fundamental equations governing the time evolution of the atmosphere. Given the broad spectrum of scales of the atmospheric phenomenon, computational limitations require parameterizations for processes not explicitly resolved at the model computational grid. The next generation of the National Aeronautics and Space Administration (NASA) Goddard Earth Observing System (GEOS) GCM is being developed as a unified, seamless model to be applied across a broad spectrum of spatial and temporal scales of the atmospheric motions. This paper provides an evaluation of relevant aspects of the GEOS forecasts across a pertinent range of horizontal resolution with an unvarying model formulation. We focus specifically on the parameterization of deep convection and evaluate its influence on model results down to the a few kilometers scale. We arrive at the unexpected conclusion that a kilometer-scale resolution where convection is mostly explicitly resolved perform worse.

## 1. Introduction

Deep atmospheric convection is a fundamental physical mechanism for heat, moisture, and momentum transfer in Earth's climate system as well as being responsible for many severe weather phenomena. Precipitating deep convective storms typically have spatial scales of tens of kilometers and lifetimes of several hours. In their infancy several decades ago, the spatial-scale resolution of atmospheric general circulation models (GCMs) was on the order of hundreds of kilometers implying convective clouds could not be explicitly resolved. As these clouds occupy a small fractional area of the model grid cell, their effects must be parameterized in terms of model-resolved variables (Arakawa, 2004; Arakawa & Schubert, 1974). Most GCMs follow this scale separation and quasi-equilibrium framework either explicitly or implicitly. Although there are other frameworks for deep convection parameterization (DPCP) as well as many others for shallow convection and cloud microphysics, it is clear that parameterized clouds and moist convection in

GCMs is a cause of bias and of uncertainty in predicting atmospheric evolution, from weather to climate time scales (Bony et al., 2015; Maher et al., 2018; Sherwood et al., 2014; Stevens & Bony, 2013; Weber & Mass, 2019).

Currently, GCMs with adequate computational resources can, in principle, be run at 1- to 10-km horizontal grid spacing, crossing the so-called “gray zone” of deep convective motions (Arakawa, 2004; Palmer & Stevens, 2019; Stevens et al., 2019). In this gray zone, a clear spatial-scale separation between subgrid-scale (SGS) convective and model-resolved motions ceases to exist. For GCMs in this gray zone, convective motions are partially resolved as they span several grid cells. In this respect, GCMs run at kilometer resolution require a scale-aware convection parameterization where the parameterization scheme is progressively damped as deep convective motions and their associated mass flux become explicitly resolved. On the other hand, the full parameterization is retained for applications requiring a much coarser spatial resolution; for example, ensemble weather forecasts, long-term predictions at seasonal scales, and ultimately century timescales or greater for climate change assessment. Given the role of deep convection in determining the nature of the atmospheric circulation and thermodynamic structure, assessing the impacts of convective parameterizations is critical and, given sufficient computational resources, is now feasible (Maher et al., 2018; Möbis & Stevens, 2012).

There has been a concerted effort within the modeling community to pursue GCMs run at spatial resolutions that reduce, or even abolish, SGS parameterizations (particularly for convection) (Marotzke et al., 2017; Palmer & Stevens, 2019; Satoh et al., 2019). In this case, the modeled equations governing atmospheric evolution would resemble the full Navier-Stokes equations. The “DYnamics of the Atmospheric general circulation Modeled On Non-hydrostatic Domains” project (Stevens et al., 2019), an intercomparison project of global “storm-resolving” models, is a particularly relevant effort toward this end. However, the exact scale at which convection parameterization is unnecessary is debatable (Hazelton et al., 2018; Petch, 2006).

Presently, running GCMs with interactive land surface, ocean, and sea ice coupling and interactive aerosols at kilometer or subkilometer scale in an operational (e.g., medium-range weather forecasting) or production (e.g., climate change assessment) framework is not viable given limitations in computational power, storage capacity, and simply analyzing output data fields (Schultheiss et al., 2019; Stevens et al., 2019). Therefore, SGS parameterizations in GCMs must be retained for some time to come and, in fact, provide a means for gauging the inherent uncertainties in representing, for example, precipitation, atmospheric circulations, and the planetary radiative budget (Maher et al., 2018). To this end, the National Aeronautics and Space Administration (NASA) Goddard Earth Observing System (GEOS) GCM is presently being developed as a unified, seamless model for applications across a broad spectrum of spatial and temporal scales. Here, and motivated by this strong push toward eliminating deep convective parameterizations, we examine precipitation, radiative balance, dynamic, and thermodynamics aspects of GEOS simulations across a range of horizontal resolutions, down to 3-km resolution, focusing on the effects of a scale-aware convective parameterization. It is important to state clearly, we do *not* intend this study to be a cautionary tale against the drive toward kilometer-scale, cloud-resolving GCMs, but rather a pathway to consider as we move in this direction.

## 2. Model Configuration and Methods

As GCMs advance toward much higher horizontal and vertical resolution, the question of the effects on model realism of removing convective parameterizations becomes extremely relevant. How to approach the elimination of the convection parameterization scheme in a systematic and replicable fashion between modeling centers is not trivial. Our approach here for assessing the scale-aware convection parameterization effects on the GEOS GCM takes advantage of the model’s seamless approach by cascading from coarser to finer resolution while maintaining, modifying, and eliminating the parameterization entirely as well as only its scale awareness capability. Here, we briefly outline the model’s basic configuration as well as describe the scale-aware DPCP.

### 2.1. GEOS GCM Model Configuration

The GEOS simulations applied the finite volume cubed-sphere nonhydrostatic dynamical core, FV3 (Putman & Lin, 2007). Here it is worth noting that FV3 does not apply explicit grid-scale diffusion for

tracers, except at a certain number of top model layers. Tracers are diffused implicitly through the tracer advection scheme or in the vertical remapping from FV3 Lagrangian to Eulerian vertical levels (Lin & Harris, 2016). Resolved grid-scale cloud microphysics applies a single-moment formulation for rain, liquid, and ice condensates (Bacmeister et al., 2006). With respect to the convection parameterization, the shallow scheme follows Park and Bretherton (2009). The scale-aware DPCP follows Freitas et al. (2018, 2020) and Grell and Freitas (2014, hereafter GF). See Text S1 (supporting information, SI) for details.

Specifically, the scale awareness within the DPCP consists of weighting the mass flux at cloud base by the factor  $(1 - \sigma)^2$ , where  $\sigma$  is the grid cell fractional area occupied by the convective clouds (Arakawa et al., 2011; Grell & Freitas, 2014). In this manner, as the model spatial resolution increases (i.e.,  $\sigma \rightarrow 1$ ), the contribution of the DPCP to the convective mass flux decreases accordingly. As in most GCMs, and of particular importance for this study, precipitation is generated by more than simply the DPCP. In GEOS, the SGS shallow convection parameterization also contributes to the precipitation. In our model experiments when both the shallow and the DPCP are retained, they are referred to as “CP”. Additionally, there is also a grid-scale component of the precipitation generated by the microphysics scheme regardless of the CP. In general, the shallow convection parameterization contribution to precipitation is small, whereas that of cloud microphysical scheme may be substantial depending on model resolution. This critical scale at which cloud microphysics and turbulent motions schemes dominate precipitation production is an open question (Bryan et al., 2003; Petch, 2006), which strongly motivates this study.

## 2.2. The Cascade of the GEOS GCM Simulations

As emphasized above, the question of spatial resolution is crucial when assessing model performance, particularly when at some given scale a critical parameterization ceases to exist. In this regard, to assess the GEOS performance with respect to DPCP, comprehensive simulations were carried out over a broad range of scales where deep convection is necessarily parameterized down to lower end of the gray zone where it may, in principle, be eliminated. Model simulations beginning on 00 UTC 20 July 2016 were run for 40 days at horizontal grid spacings of approximately 100, 50, 25, 12, 6, and 3 km, formally referred to as C0090, C0180, C0360, C0720, C1440, and C2880, respectively. The European Centre for Medium-Range Weather Forecasts (ECMWF) ERA-5 global reanalysis (Hersbach et al., 2019) provided the initial atmospheric conditions, while sea surface temperatures were prescribed following Reynolds et al. (2002). Results from the last 30 days form the basis for the analysis and discussion presented here.

Specifically, in order to directly assess DPCP influence at convection-resolving regimes (at 3 km), two additional experiments were performed:

1. eliminating the DPCP entirely, hereafter “noDP”
2. and applying the DPCP without GF scale awareness approach, “noSA.”

These latter experiments provide insight into the grid-scale and SGS convective cloud representations in GEOS and shed light on the impact of the DPCP at convection-permitting model configurations.

## 3. Results and Discussions

Here, we provide an evaluation of the cascading runs, focusing on metrics commonly employed for assessing GCMs, such as precipitation characteristics (spatial pattern, diurnal cycle, and sensitivity to environmental moisture), radiative balance, and atmospheric dynamic and thermodynamic state. See Text S2 (SI) for the observational and reanalysis data utilized for this goal.

### 3.1. Model Resolution: Effects on Spatial and Temporal Variability of Precipitation

Figures 1a1 and 1a2 display monthly mean precipitation for August 2016 as estimated by GPCP and GPM, respectively. The spatial precipitation patterns are remarkably similar in location and mean intensity, with global areal means of 2.77 and 3.13 mm day<sup>-1</sup>. The remaining panels (b through g) display GEOS-simulated precipitation fields. Total precipitation (left-hand side) is defined by summing CP-generated and microphysics-generated precipitation. Total precipitation due solely to the CP appears on the right-hand side. Model resolution, from top to bottom, increases from C0090 (~100 km) to C2880 (~3 km). At the lowest resolution (Figures 1b1 and 1b2), tropical rainfall is, not surprisingly, predominately attributable to CP while the cloud and precipitation microphysics scheme dominates at higher latitudes. The simulated global total

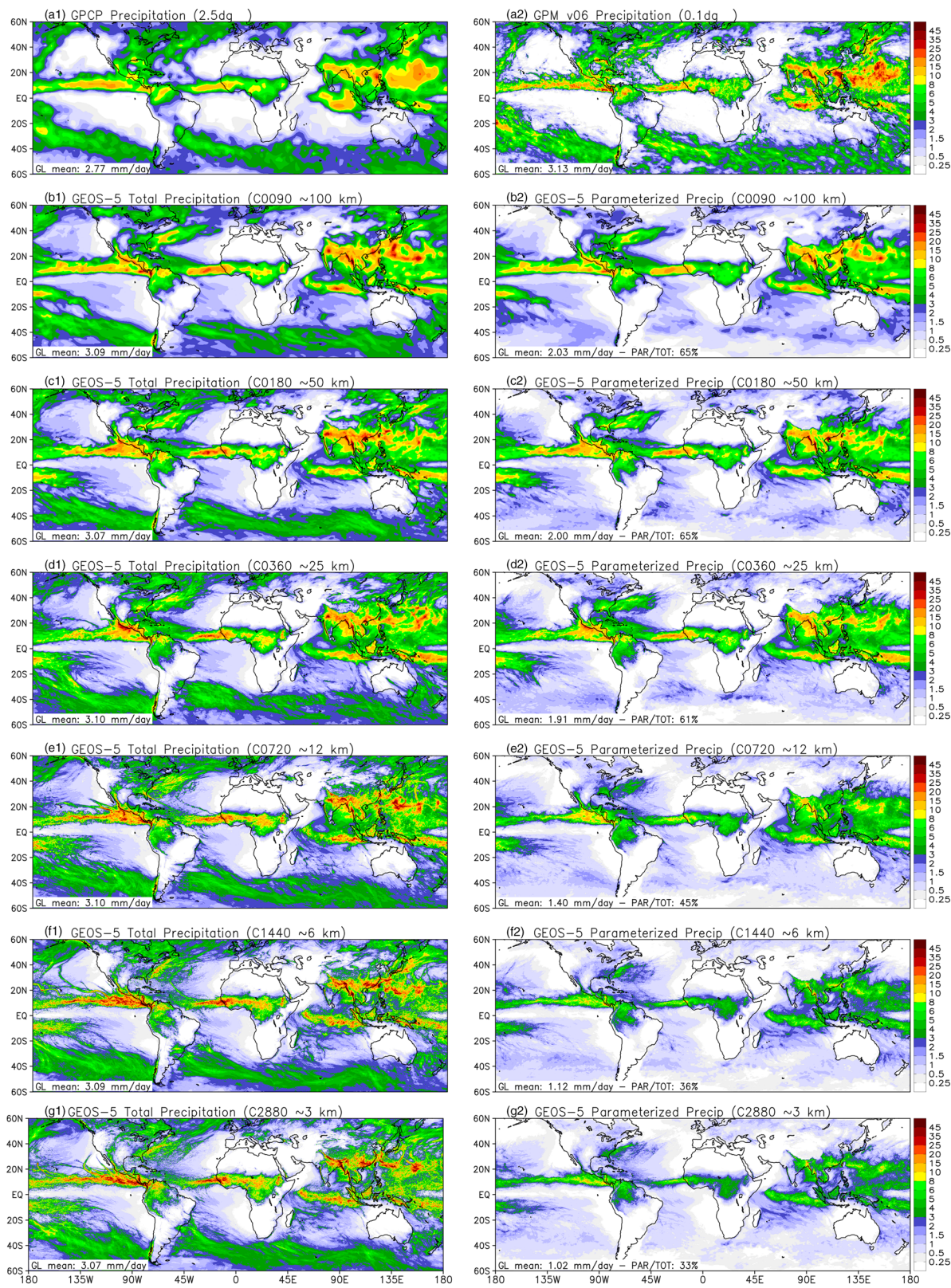


**Figure 1.** August 2016 precipitation mean ( $\text{mm day}^{-1}$ ) as estimated by GPCP and GPM (a1 and a2, respectively). The remaining panels show the GEOS GCM simulated total precipitation (left-hand side) and by its convection parameterization only (right-hand side). From top to bottom (b–g), model resolution increases from C0090 (~100 km) to C2880 (~3 km). The global areal mean of each precipitation case appears on the left bottom of each panel.

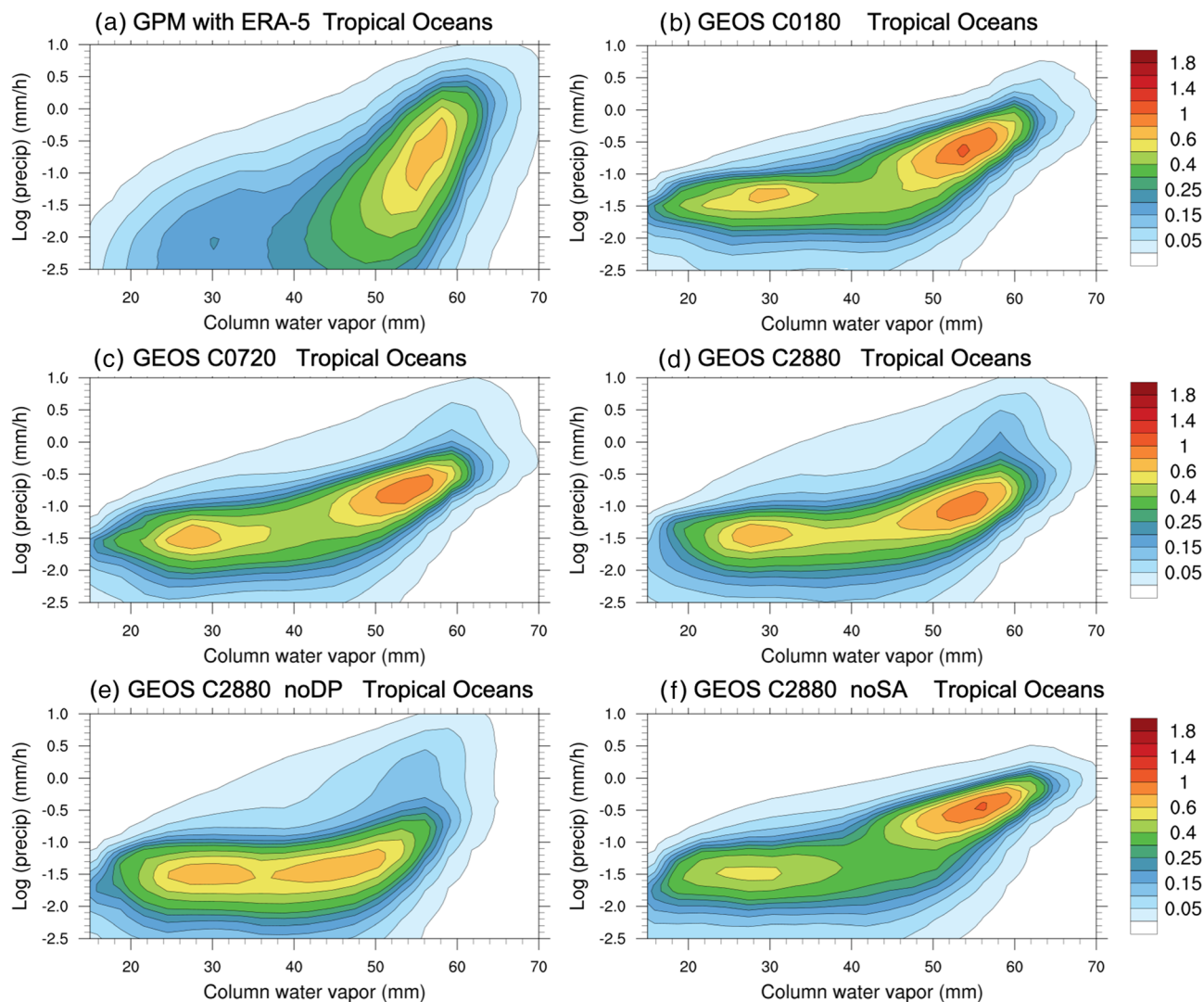


**Figure 2.** Bivariate joint probability density function (PDF) between the column water vapor (CWV, mm) and the logarithm of the precipitation rate ( $\text{mm hr}^{-1}$ ). The analysis is limited to the tropical oceanic regions enclosed by the latitude 20°S to 20°N. (a) PDF of GPM precipitation versus ERA-5 CWV. The correspondent PDF of GEOS are shown at horizontal resolutions of (b) C0180, (c) C0720, and (d) C2880. The remaining panels depict the PDF associated with the extreme cases (e) noDP, and (f) noSA of application of the GF deep convection parameterization.

precipitation pattern, 65% of which is attributable to the CP, closely resembles those of GPCP and GPM, with global mean of  $3.09 \text{ mm day}^{-1}$ . As the resolution increases, the global mean precipitation ranges between  $3.07$  and  $3.10 \text{ mm/day}$ , falling between the GPCP and GPM estimates. At these higher resolutions, the microphysics scheme gains prominence over the CP-produced precipitation and total precipitation field becomes richer in detail with filamentary structures. The CP precipitation contribution to global mean decreases monotonically from  $2.03 \text{ mm day}^{-1}$  (65% of the total of  $3.09 \text{ mm/day}$ ) at C0090 to  $1.02 \text{ mm day}^{-1}$  (33% of the total of  $3.07 \text{ mm/day}$ ) at C2880. Notably, from C0360 to C0720 and then to C1440, the scale awareness approach produces sudden jumps in the total precipitation partition (Figure S2a).

At C2880 resolution, the noDP/noSA experiments (Figure S1, SI) reveal a slight increase/decrease in total precipitation from  $3.07$  to  $3.11/2.99 \text{ mm day}^{-1}$ , while the CP-generated precipitation decreases/increases from  $1.02$  to  $0.62/1.79 \text{ mm day}^{-1}$ . When the DPCP is eliminated entirely, the shallow convection scheme precipitation becomes more prominent.

Faithfully reproducing the diurnal cycle of precipitation has long challenged convection parameterizations (Betts & Jakob, 2002, Bechtold et al., 2014, among many others). Figure S2a (SI) presents both the GPM and GEOS-simulated diurnal cycle of precipitation. The GPM diurnal cycle of precipitation produces two well-defined peaks: a nocturnal peak over oceanic regions and a late-afternoon peak over land. Across scales, the amplitude of the GEOS mean precipitation overestimates GPM by about 8%, while the phase agrees relatively well between the two. The CP precipitation mean amplitude monotonically decreases with increased resolution, as discussed above. Regarding the phase, the peak of the GEOS precipitation over land closely approximating GPM at lower resolutions and steadily regresses toward local noon as resolution increases.

Figure S2b (SI) presents results where the DPCP is turned off or its scale awareness is eliminated; that is, noDP and noSA, respectively. For the noDP experiment, CP-generated precipitation is solely associated with the shallow convection parameterization, as already stated. In the experiment noSA, the CP precipitation is much more pronounced, as expected, with better phase agreement compared with the noDP experiment.

A critical variable related to the temporal evolution and intensity of deep convective precipitation particularly in the tropics is column, or precipitable, water vapor (CWV) (e.g., Adams et al. (2013, 2017), Ahmed & Schumacher (2015), Bretherton et al. (2004), Holloway & Neelin (2009), Kuo et al. (2020), Lintner et al. (2017), Stevens et al. (2019)). We combined the August 2016 GPM daily mean precipitation rate at 0.1° with the daily mean CWV from ERA-5 global reanalysis after regridding onto the GPM grid resolution. Figure 2a shows the bivariate joint probability density function (PDF) for CWV (mm) and the logarithm of the precipitation rate in  $\text{mm hr}^{-1}$  for tropical (20 S to 20 N) oceanic regions; the accumulated PDF amounting to 100%. The GPM precipitation shows a remarkable dependence on CWV, sharply increasing the rainfall intensity (about 3 orders of magnitude) between CWV values between 50 and 60 mm. Precipitation is suppressed for CWV values above 65 to 70 mm. At lower CWV values, both rainfall intensity and the probability of occurrence are also much less pronounced, although this may reflect the underestimation of light rain events by the GPM (Xu et al., 2017). In general, these results are consistent with those reported by Bretherton et al. (2004) and Rushley et al. (2018), over tropical oceans, and by Schiro et al. (2016), over tropical land.

The GEOS precipitation-CWV relationship, for the same spatial domain and time averaging of the GPM/ERA-5 analysis, is shown in Figure 2b at C0180, Figure 2c at C0720, and Figure 2d at C2880 resolutions. GEOS also produces increased rainfall intensity with CWV for values between 50 to 60 mm, though not as sharp as with GPM/ERA-5 data, implying weakened sensitivity to environmental moisture. Rushley et al. (2018) evaluated this relationship for 28 models in the Coupled Model Intercomparison Project, Phase 5 (CMIP5), finding similar behavior. Across model resolutions, GEOS fails to produce extreme precipitation events as frequently as GPM. Also, GEOS PDFs are dipole in nature, with an additional local maximum in the lower range of CWV (<40 mm) at very small precipitation amounts ( $<10^{-3} \text{ mm hr}^{-1}$ ), not evident in the GPM/ERA-5 data. Furthermore, as resolution increases, model results show lesser dependence on column moisture, with the increase of precipitation with CWV becoming smoother and the two peaks less distinct. On the other hand, precipitation suppression in the model occurs at lower values of CWV. An additional 12-km resolution simulation (not shown), only differing in the application of a two-moment cloud microphysics scheme (Barahona et al., 2014), resembles the PDF of Figure 2c, indicating the dominance of the CP in determining the PDF.

Recently, Kuo et al. (2020) analyzed similar relationships for 20 models' configurations. Most of the models simulated, to some degree, the observed precipitation increases with increasing CWV. The principal discrepancies in model results were tied to different convection parameterizations. Also, individual model case studies where the differences were mostly associated with time and space resolution or cloud microphysics formulations revealed similar statistics. Additionally, these authors found an excess of light precipitation at lower CWV values, also consistent with our simulations.

In terms of the experiments evaluating the effects of the CP, disabling the DPCP (Figure 2e, noDP) resulted in the poorest results, with the precipitation PDF being fairly insensitive to CWV, and greater precipitation at intermediate CWV values (30–40 mm). In this case, the precipitation suppression occurs at even lower CWV. In the other extreme case, applying the CP without scale awareness (Figure 2f, noSA) considerably improves model results, with the precipitation PDF exhibiting greater moisture sensitivity as well as decreasing precipitation amounts at lower CWV values.

In the same spirit as our study, Bryan et al. (2003) and Bryan and Morrison (2012) examined the resolution dependence on simulating deep convection, without CP, in limited area model domains. Their series of simulations from 4 km down to 125-m resolution revealed significant discrepancies. Those differences were attributed to the ability of the higher resolutions (subkilometer) runs to become turbulent whereby updraft entrainment is resolved. Their kilometer-scale runs produced relatively more laminar ascending flows (see Figure 1 of Bryan et al., 2003). More recently, Lebo and Morrison (2015) investigated the effects of model grid box lengths on mixing in Squall Lines simulations. From a comprehensive set of simulations with a limited area model and horizontal grid spacing ( $\Delta h$ ) varying from  $\sim 33$  m to 2 km, they concluded that entrainment and detrainment are suppressed with  $\Delta h > 500$  m.

In GF DPCP, as with any CP, a lateral mixing formulation (entrainment) is always present to account for the turbulent mixing process between cloud updrafts and the environment. In the context of our runs, we speculate that grid-scale horizontal mixing in GEOS is underestimated, with resolved plumes retaining their initial buoyancy and causing convection to occur more easily with almost no sensitivity to the environmental moisture.

### 3.2. Top of the Atmosphere Radiative Budget

Given that deep convection is a fundamental mechanism for vertical energy transport, it is important to consider the atmospheric energy budget, specifically top of the atmosphere (TOA) radiative budget. Figure S3 (SI) shows the zonal monthly mean TOA longwave (LW) and shortwave (SW) radiative fluxes from CERES-EBAF and GEOS simulations. Across model resolutions (Figures S3a and S3b), at higher latitudes, GEOS always underestimates/overestimates the TOA LW/SW fluxes. These discrepancies result from excess total water condensate in comparison with ERA-5 (not shown). Between latitude 30°S and 30°N, the radiative fluxes have larger variation and greater discrepancies with CERES-EBAF with increasing resolution. Considering the global mean, from C0180 to C2880, the LW changes from 244.0 to 245.8  $\text{W m}^{-2}$ , or 2.2 to 4  $\text{W m}^{-2}$  above CERES-EBAF values. On the other hand, the SW changes from 95.2 to 86.8  $\text{W m}^{-2}$ , or 0.3 to  $-8.1 \text{ W m}^{-2}$ . The noDP case (Figures S3c and S3d) differed from the observed values of LW/SW by 5.4/ $-9.3 \text{ W m}^{-2}$  respectively, while the noSA case differed by only 0.8/ $-5.3 \text{ W m}^{-2}$ .

### 3.3. Atmospheric Dynamic and Thermodynamic State

Here we evaluate the model atmospheric state using ERA-5 reanalysis as the reference dataset. Figure S4 (SI) depicts the global monthly mean vertical profiles of mean error (BIAS) and the root-mean-square error (RMSE) for temperature, water vapor mixing ratio, and zonal wind. From C0180 to C2880 (Figure S4a), the model bias in water vapor in the free troposphere changes from a vertically balanced condition (mostly dry/wet below/above 700 hPa) to a uniformly drier condition in the entire column. The noDP case (Figure S4d) has the highest dry bias, while the noSA case restores more vertically balanced conditions. In terms of RMSE, all experiments reveal the largest discrepancies in the lower troposphere and the noDP case gives the least satisfactory results.

The temperature bias (Figure S4b) shows greater variability, exhibiting colder and warmer vertical layers. Between 900 and 250 hPa, the noSA (Figure S4e) experiment has a considerable warm bias. The RMSE for noDP and the C2880 run are largest ( $\sim 2$  K) and confined to the upper troposphere. The spatial distribution of the bias (Figure S5, SI) reveals further details about model performance. For example, from C0180 to C2880 the warm bias at 100 hPa in the tropics steadily increases from  $\sim 1$  to 2 K and increases further to  $\sim 2$  to 3 K in the noDP case, while decreasing to  $\sim 1$  K in the noSA case. At higher northern latitudes, a warmer layer from the surface up to 300 hPa followed by a colder layer extending to upper levels is present in all simulations. The noDP case shows by far the larger warm bias up to  $\sim 6$  K (Figure S5e).

From the near-surface level to approximately 600 hPa, all simulations have comparable U-zonal wind biases (Figure S4c). Subsequently, all the simulations gradually diverge upward, with the mean error increasing with increased resolution. Perhaps unanticipated, the U-zonal biases of the two extreme DPCP cases (Figure S4f) lie at the edges of the model bias range, with the noDP/noSA case performing the worst/best.

To further examine details on how accurately zonal circulations are simulated, Figure 3 shows the latitude-pressure cross sections of the monthly mean zonal average of the U-zonal wind component. Figure 3a shows the ERA-5 data in which there are two distinct westerly subtropical jets around 200 hPa,

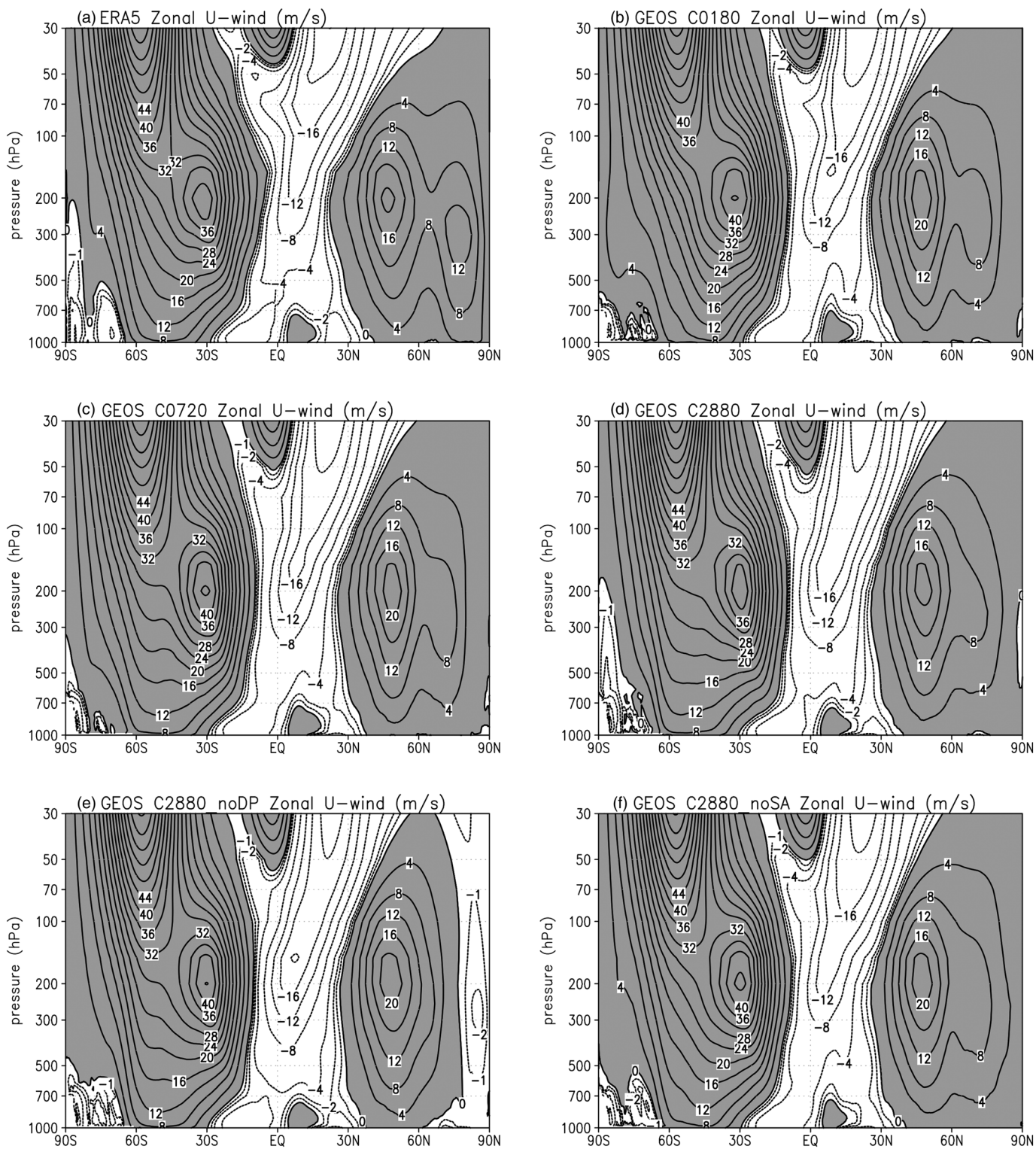


**Figure 3.** Latitude-pressure cross section of zonal average of the horizontal wind component for August 2016. Pressure is plotted on logarithmic scale. Contours interval is  $4 \text{ m s}^{-1}$ ; westerly values are shaded. Panel (a) shows the ERA-5 reanalysis data used here as a reference for the model simulations. The remaining panels show the GEOS GCM simulations at horizontal resolutions of (b) C0180, (c) C0720, (d) C2880, plus (e) C2880 without the GF deep convection parameterization, and (f) C2880 without the GF scale awareness approach.

surrounding tropical easterly flow of  $\sim 12 \text{ m s}^{-1}$ . Furthermore, at northern high latitudes around 300 hPa, the westerly polar jet is very apparent. Figures 3b–3d show model results at C0180, C0720, and C2880. In general, GEOS reproduced the circulation patterns across these resolutions fairly well, however, with several discrepancies. From C0180 to C2880, there is a tendency to weaken the polar jet, while strengthening the tropical, upper troposphere easterly current approximately  $4 \text{ m s}^{-1}$  (note the downward shift of the  $-16 \text{ m s}^{-1}$  contour line).

Concerning these two extreme cases, noDP (Figure 3e) differs even more radically from the expected patterns, curiously reversing the Arctic zonal circulation, the polar and subtropical jets are blended, and tropical easterly flow is further exaggerated. However, Figure 3f demonstrates that the noSA case strengthens the polar westerly jet and restores the upper troposphere tropical easterly flow to its expected configuration, closely resembling the ERA-5 circulations. The reasons for the model's behavior are unclear. However, as many CPs, the GF DPCP, also includes SGS convective momentum transport (CMT), and the current formulation, restricts it to be downgradient. It is well established that the inclusion of CMT helps GCMs to reproduce the atmospheric circulation. For example, Richter and Rasch (2008) reported that CMT improved the representation of the Hadley circulation and reduced biases in the tropical easterly and subtropical westerly jets in the Community Atmosphere Model, Version 3 (CAM3). One caveat here is that CAM3 ran with a resolution of  $1.9 \times 2.5^\circ$ , whereas our GEOS-5 performance refers to a much higher spatial resolution.

#### 4. Conclusion

We have presented an overview of the performance of the NASA GEOS GCM simulations down a cascade of horizontal resolutions. Across these resolutions, model formulation was unvarying. However, to assess the viability of moving toward a very high resolution (3 km) GCMs without DPCP, two additional runs were carried out.

As a rule, DPCP impacts are gradually damped by its scale awareness approach with increasing resolution, leaving dynamics and the cloud microphysics scheme to dominate convective rainfall production and its associated myriad upscale impacts. As a consequence, across resolutions the convective precipitation smoothly transitions from being mainly produced by the SGS to the grid-scale model components with the generated monthly mean total precipitation, both in intensity and spatial distribution, remaining nearly invariable. Likewise, the simulated mean atmospheric temperature, water vapor, and horizontal wind components showed internal consistency resembling ERA-5 reanalysis across model resolutions.

However, our analysis also indicated model deficiencies, for example; the precipitation rate's reduced sensitivity to ambient moisture with increased resolution and nearly complete insensitivity at the highest resolution (3 km) when DPCP is completely turned off (Figure 2e). Although somewhat speculative, we attribute this discrepancy to underestimation of horizontal mixing.

For the noSA case (Figure 2f), model performance is improved given that SGS horizontal mixing represented by the lateral entrainment formulation of the DPCP is retained. Future research will test this hypothesis through adding an explicit, grid-scale horizontal mixing for tracers in GEOS GCM.

A second deficiency is the degradation of the zonal circulation. Without the DPCP, the model performed poorly, blending the upper-tropospheric northern westerly jets and inverting the Arctic zonal circulation. Even at kilometer scales, resolved deep convective motions and cloud processes resulting from the cloud microphysics scheme fail to properly distribute the latent heating in space and, consequently, modify the pressure field, which ultimately drives the atmospheric motion. When the DPCP is turned on, the results are much improved, implying a more accurate distribution of latent heating and resulting atmospheric circulation response.

Though the GCM community has expressed the desire to eliminate DPCP entirely, our results indicate some need for caution as we move toward the goal of a kilometer- or subkilometer-scale resolution. At least for GEOS, it appears that either changes in the dynamics are required to increase the inhibition of explicit convection, or some form of scale-aware, DPCP must be maintained even at kilometer resolution.

However, it must remain crystal clear that we are not arguing against the drive toward higher-resolution numerical models for both weather and climate prediction. We understand that, while both parameterized

and explicit (but poorly resolved) convection have deficiencies, the nature of a parameterization allows it to be tuned. In contrast, explicit convection problems are more difficult to fix because there are no readily parameters to adjust. We expect certain phenomena, like mesoscale convective systems, to be better simulated in a convective resolving models, but a model climatology and skillful forecasts are very sensitive to tuning, and the parameterized convection benefits from a longer history of application and development.

## Data Availability Statement

The GEOS GCM data simulations are available on the NASA data portal (<https://portal.nccs.nasa.gov/data-share/DYAMOND/>).

## Acknowledgments

S. R. Freitas acknowledges the funding by the Cooperative Agreement NASA/GSFC - USRA/GESTAR: NNG11HP16A. D. K. Adams contributed to this study during a yearlong sabbatical at Rutgers University with funding from Programa de Apoyos para la Superación del Personal Académico de la UNAM (PASPA). The authors acknowledge the availability of the following data sets:

- a. CERES-EBAF (<https://ceres.larc.nasa.gov/products.php?product=EBAF-TOA>)
- a. ERA-5 (<https://cds.climate.copernicus.eu/cdssapp#!/dataset/reanalysis-era5-pressure-levels?tab=overview>)
- a. GPM (<https://pmmm.nasa.gov/data-access/downloads/gpm>)
- a. GPCP (<https://www.esrl.noaa.gov/psd/data/gridded/data.gpcp.html>).

## References

- Adams, D. K., Barbosa, H. M. J., & De Los Rios, K. (2017). A spatiotemporal water vapor/deep convection correlation metric derived from the Amazon Dense GNSS Meteorological Network. *Monthly Weather Review*, 145(1), 279–288. <https://doi.org/10.1175/MWR-D-16-0140.1>
- Adams, D. K., Gutman, S., Holub, K., & Pereira, D. (2013). GNSS observations of deep convective timescales in the Amazon. *Geophysical Research Letters*, 40, 2818–2823. <https://doi.org/10.1002/grl.50573>
- Ahmed, F., & Schumacher, C. (2015). Convective and stratiform components of the moisture precipitation relationship. *Geophysical Research Letters*, 42, 10,453–10,462. <https://doi.org/10.1002/2015GL066957>
- Arakawa, A. (2004). The cumulus parameterization problem: Past, present, and future. *Journal of Climate*, 17(13), 2493–2525. [https://doi.org/10.1175/1520-0442\(2004\)017%3C2493:RATCPP%3E2.0.CO;2](https://doi.org/10.1175/1520-0442(2004)017%3C2493:RATCPP%3E2.0.CO;2)
- Arakawa, A., Jung, J.-H., & Wu, C.-M. (2011). Toward unification of the multiscale modeling of the atmosphere. *Atmospheric Chemistry and Physics*, 11(8), 3731–3742. <https://doi.org/10.5194/acp-11-3731-2011>
- Arakawa, A., & Schubert, W. H. (1974). Interaction of a cumulus cloud ensemble with the large-scale environment. Part I. *Journal of the Atmospheric Sciences*, 31(3), 674–701. [https://doi.org/10.1175/1520-0469\(1974\)031%3C0674:IOACCE%3E2.0.CO;2](https://doi.org/10.1175/1520-0469(1974)031%3C0674:IOACCE%3E2.0.CO;2)
- Bacmeister, J. T., Suarez, M. J., & Robertson, F. R. (2006). Rain reevaporation, boundary layer-convection interactions, and Pacific rainfall patterns in a AGCM. *Journal of the Atmospheric Sciences*, 63(12), 3383–3403. <https://doi.org/10.1175/JAS3791.1>
- Barahona, D., Molod, A., Bacmeister, J., Nenes, A., Gettelman, A., Morrison, H., et al. (2014). Development of two-moment cloud micro-physics for liquid and ice within the NASA Goddard Earth Observing System Model (GEOS-5). *Geoscientific Model Development*, 7(4), 1733–1766. <https://doi.org/10.5194/gmd-7-1733-2014>
- Bechtold, P., Semane, N., & Lopez, P. (2014). Representing equilibrium and nonequilibrium convection in large-scale models. *Journal of the Atmospheric Sciences*, 71(2), 734–753. <https://doi.org/10.1175/JAS-D-13-0163.1>
- Betts, A. K., & Jakob, C. (2002). Evaluation of the diurnal cycle of precipitation, surface thermodynamics, and surface fluxes in the ECMWF model using LBA data. *Journal of Geophysical Research*, 107(D20), 8045. <https://doi.org/10.1029/2001JD000427>
- Bony, S., Stevens, B., Frierson, D. M. W., Jakob, C., Kageyama, M., Pincus, R., et al. (2015). Clouds, circulation and climate sensitivity. *Nature Geoscience*, 8(4), 261–268. <https://doi.org/10.1038/ngeo2398>
- Bretherton, C. S., Peters, M. E., & Back, L. E. (2004). Relationships between water vapor path and precipitation over the tropical oceans. *Journal of Climate*, 17(7), 1517–1528. [https://doi.org/10.1175/1520-0442\(2004\)017%3C1517:RBWVPA%3E2.0.CO;2](https://doi.org/10.1175/1520-0442(2004)017%3C1517:RBWVPA%3E2.0.CO;2)
- Bryan, G. H., & Morrison, H. (2012). Sensitivity of a simulated squall line to horizontal resolution and parameterization of microphysics. *Monthly Weather Review*, 140(1), 202–225. <https://doi.org/10.1175/MWR-D-11-00046.1>
- Bryan, G. H., Wyngaard, J. C., & Fritsch, J. M. (2003). Resolution requirements for the simulation of deep moist convection. *Monthly Weather Review*, 131(10), 2394–2416. [https://doi.org/10.1175/1520-0493\(2003\)131%3C2394:RRFTSO%3E2.0.CO;2](https://doi.org/10.1175/1520-0493(2003)131%3C2394:RRFTSO%3E2.0.CO;2)
- Freitas, S. R., Grell, G. A., & Li, H. (2020). The GF convection parameterization: Recent developments, extensions, and applications. *Geoscientific Model Development Discussion*. <https://doi.org/10.5194/gmd-2020-38>
- Freitas, S. R., Grell, G. A., Molod, A., Thompson, M. A., Putman, W. M., Santos E Silva, C. M., & Souza, E. P. (2018). Assessing the Grell-Freitas convection parameterization in the NASA GEOS modeling system. *Journal of Advances in Modeling Earth Systems*, 10, 1266–1289. <https://doi.org/10.1029/2017MS001251>
- Grell, G. A., & Freitas, S. R. (2014). A scale and aerosol aware stochastic convection parameterization for weather and air quality modeling. *Atmospheric Chemistry and Physics*, 14(10), 5233–5250. <https://doi.org/10.5194/acp-14-5233-2014>
- Hazelton, A. T., Harris, L., & Lin, S. J. (2018). Evaluation of tropical cyclone structure forecasts in a high-resolution version of the multi-scale GFDL fvGFS model. *Weather and Forecasting*, 33(2), 419–442. <https://doi.org/10.1175/WAF-D-17-0140.1>
- Hersbach, H., Bell, W., Berrisford, P., Horányi, A., Muñoz Sabater, J., Nicolas, J., et al. (2019). Global reanalysis: Goodbye ERA-Interim, hello ERA5. *ECMWF Newsletter*, 159, 17–24. <https://doi.org/10.21957/vf291hehd7>
- Holloway, C. E., & Neelin, J. D. (2009). Moisture vertical structure, column water vapor and tropical deep convection. *Journal of the Atmospheric Sciences*, 66(6), 1665–1683. <https://doi.org/10.1175/2008JAS2806>
- Kuo, Y., Neelin, J. D., Chen, C., Chen, W., Donner, L. J., Gettelman, A., et al. (2020). Convective transition statistics over tropical oceans for climate model diagnostics: GCM evaluation. *Journal of the Atmospheric Sciences*, 77(1), 379–403. <https://doi.org/10.1175/JAS-D-19-0132.1>
- Lebo, Z. J., & Morrison, H. (2015). Effects of horizontal and vertical grid spacing on mixing in simulated squall lines and implications for convective strength and structure. *Monthly Weather Review*, 143(11), 4355–4375. <https://doi.org/10.1175/MWR-D-15-0154.1>
- Lin, S. J., & Harris, L. (2016). Explicit Diffusion in GFDL FV3. [https://www.gfdl.noaa.gov/wp-content/uploads/2017/09/Diffusion\\_operators.pdf](https://www.gfdl.noaa.gov/wp-content/uploads/2017/09/Diffusion_operators.pdf)
- Lintner, B. D., Adams, K., Schiro, K. A., Stansfield, A., da Rocha, A., & Neelin, J. D. (2017). Relationships among climatological moisture vertical structure, column water vapor, and precipitation over the central Amazon in observations and CMIP5 models. *Geophysical Research Letters*, 44, 1981–1989. <https://doi.org/10.1002/2016GL071923>

- Maher, P., Vallis, G. K., Sherwood, S. C., Webb, M. J., & Sansom, P. G. (2018). The impact of parameterized convection on climatological precipitation in atmospheric global climate models. *Geophysical Research Letters*, 45, 3728–3736. <https://doi.org/10.1002/2017GL076826>
- Marotzke, J., Jakob, C., Bony, S., Dirmeyer, P. A., O'Gorman, P. A., Hawkins, E., et al. (2017). Climate research must sharpen its view. *Nature Climate Change*, 7(2), 89–91. <https://doi.org/10.1038/nclimate3206>
- Möbis, B., & Stevens, B. (2012). Factors controlling the position of the Intertropical Convergence Zone on an aquaplanet. *Journal of Advances in Modeling Earth Systems*, 4, M00A04. <https://doi.org/10.1029/2012MS000199>
- Palmer, T., & Stevens, B. (2019). The scientific challenge of understanding and estimating climate change. *Proceedings of the National Academy of Sciences*, 116(49), 24,390–24,395. <https://doi.org/10.1073/pnas.1906691116>
- Park, S., & Bretherton, C. S. (2009). The University of Washington shallow convection and moist turbulence schemes and their impact on climate simulations with the community atmosphere model. *Journal of Climate*, 22(12), 3449–3469. <https://doi.org/10.1175/2008JCLI2557.1>
- Petch, J. C. (2006). Sensitivity studies of developing convection in a cloud-resolving model. *Quarterly Journal of the Royal Meteorological Society*, 132(615), 345–358. <https://doi.org/10.1256/qj.05.71>
- Putman, W., & Lin, S.-J. (2007). Finite volume transport on various cubed sphere grids. *Journal of Computational Physics*, 227(1), 55–78. <https://doi.org/10.1016/j.jcp.2007.07.022>
- Reynolds, R. W., Rayner, N. A., Smith, T. M., Stokes, D. C., & Wang, W. (2002). An improved in situ and satellite SST analysis for climate. *Journal of Climate*, 15(13), 1609–1625. [https://doi.org/10.1175/1520-0442\(2002\)015%3C1609:AIISAS%3E2.0.CO;2](https://doi.org/10.1175/1520-0442(2002)015%3C1609:AIISAS%3E2.0.CO;2)
- Richter, J. H., & Rasch, P. J. (2008). Effects of convective momentum transport on the atmospheric circulation in the community atmosphere model, version 3. *Journal of Climate*, 21(7), 1487–1499. <https://doi.org/10.1175/2007JCLI1789.1>
- Rushley, S. S., Kim, D., Bretherton, C. S., & Ahn, M.-S. (2018). Reexamining the nonlinear moisture-precipitation relationship over the tropical oceans. *Geophysical Research Letters*, 45, 1133–1140. <https://doi.org/10.1002/2017GL076296>
- Satoh, M., Stevens, B., Judt, F., Khairoutdinov, M., Lin, S. J., Putman, W. M., & Düben, P. (2019). Global cloud-resolving models. *Current Climate Change Report*, 5(3), 172–184. <https://doi.org/10.1007/s40641-019-00131-0>
- Schiavo, K. A., Neelin, J. D., Adams, D. K., & Lintner, B. R. (2016). Deep convection and column water vapor over tropical land versus tropical ocean: A comparison between the Amazon and the tropical Western Pacific. *Journal of the Atmospheric Sciences*, 73(10), 4043–4063. <https://doi.org/10.1175/JAS-D-16-0119.1>
- Schluthess, T. C., Bauer, P., Wedi, N., Fuhrer, O., Hoefler, T., & Schär, C. (2019). Reflecting on the goal and baseline for exascale computing: A roadmap based on weather and climate simulations. *Computing in Science & Engineering*, 21(1), 30–41. <https://doi.org/10.1109/MCSE.2018.2888788>
- Sherwood, S. C., Bony, S., & Dufresne, J.-L. (2014). Spread in model climate sensitivity traced to atmospheric convective mixing. *Nature*, 505(7481), 37–42. <https://doi.org/10.1038/nature12829>
- Stevens, B., & Bony, S. (2013). What are climate models missing. *Science*, 340(6136), 1053–1054. <https://doi.org/10.1126/science.1237554>
- Stevens, B., Satoh, M., Auger, L., Biercamp, J., Bretherton, C. S., Chen, X., et al. (2019). DYAMOND: The DYnamics of the Atmospheric general circulation Modeled On Non-hydrostatic Domains. *Progress in Earth and Planetary Science*, 6(1), 61. <https://doi.org/10.1186/s40645-019-0304-z>
- Weber, N. J., & Mass, C. F. (2019). Sub-seasonal weather prediction in a global convection-permitting model. *Bulletin of the American Meteorological Society*, 100(6), 1079–1089. <https://doi.org/10.1175/BAMS-D-18-0210.1>
- Xu, R., Tian, F., Yang, L., Hu, H., Lu, H., & Hou, A. (2017). Ground validation of GPM IMERG and TRMM 3B42V7 rainfall products over southern Tibetan Plateau based on a high-density rain gauge network. *Journal of Geophysical Research: Atmospheres*, 122, 910–924. <https://doi.org/10.1002/2016JD025418>

## References From the Supporting Information

- Adler, R. F., Huffman, G. J., Chang, A., Ferraro, R., Xie, P., Janowiak, J., et al. (2003). The version-2 Global Precipitation Climatology Project (GPCP) monthly precipitation analysis (1979–present). *Journal of Hydrometeorology*, 4(6), 1147–1167. [https://doi.org/10.1175/1525-7541\(2003\)004<1147:TVGPCP>2.0.CO;2](https://doi.org/10.1175/1525-7541(2003)004<1147:TVGPCP>2.0.CO;2)
- Bretherton, C. S., & Park, S. (2009). A new moist turbulence parameterization in the community atmosphere model. *Journal of Climate*, 22(12), 3422–3448. <https://doi.org/10.1175/2008JCLI2556.1>
- Huffman, G. J., Bolvin, D. T., Braithwaite, D., Hsu, K., Joyce, R., Kidd, C., et al. (2019). Algorithm Theoretical Basis Document (ATBD) version 5.2 for the NASA Global Precipitation Measurement (GPM) Integrated Multi-satellite Retrievals for GPM (I-MERG), GPM Project, Greenbelt, MD, 38 pp. [https://pmm.nasa.gov/sites/default/files/document\\_files/IMERG\\_ATBD\\_V6.pdf](https://pmm.nasa.gov/sites/default/files/document_files/IMERG_ATBD_V6.pdf)
- Iacono, M. J., Delamere, J. S., Mlawer, E. J., Shephard, M. W., Clough, S. A., & Collins, W. D. (2008). Radiative forcing by long-lived greenhouse gases: Calculations with the AER radiative transfer models. *Journal of Geophysical Research*, 113, D13103. <https://doi.org/10.1029/2008JD009944>
- Lock, A. P., Brown, A. R., Bush, M. R., Martin, G. M., & Smith, R. N. B. (2000). A new boundary layer mixing scheme. Part I: Scheme description and single-column model tests. *Monthly Weather Review*, 128(9), 3187–3199. [https://doi.org/10.1175/1520-0493\(2000\)128%3C3187:ANBLMS%3E2.0.CO;2](https://doi.org/10.1175/1520-0493(2000)128%3C3187:ANBLMS%3E2.0.CO;2)
- Loeb, N. G., Doelling, D. R., Wang, H., Su, W., Nguyen, C., Corbett, J. G., et al. (2018). Clouds and the Earth's Radiant Energy System (CERES) Energy Balanced and Filled (EBAF) Top-of-Atmosphere (TOA) edition-4.0 data product. *Journal of Climate*, 31(2), 895–918. <https://doi.org/10.1175/JCLI-D-17-0208.1>
- Louis, J., & Geleyn, J. (1982). A short history of the PBL parameterization at ECMWF. Proc. ECMWF Workshop on Planetary Boundary Layer Parameterization, Reading, United Kingdom, ECMWF, 5980.